Calculations on the adsorption of Au to MgO surfaces using SIESTA

Rudy Coquet, Graham J. Hutchings, Stuart H. Taylor and David J. Willock*

Received 25th January 2006, Accepted 23rd March 2006
First published as an Advance Article on the web 12th April 2006
DOI: 10.1039/b601213b

The SIESTA suite of programs allows periodic density functional theory calculations to be carried out on system sizes of several hundred atoms. Here we make use of this to study the interface between Au and MgO surfaces. Atomic Au on MgO(100) shows preferential binding over surface anion sites, while the binding energy at a surface anion vacancy is significantly higher than on the stoichiometric surface. High index surfaces are used to generate kink site structures representative of extended defects and Au adsorption at these sites has a binding energy intermediate between MgO(100) and the anion vacancy. In contrast Au_{10} clusters are found to bind more strongly to kink sites than anion vacancies. Bader charge analysis demonstrates that electron transfer occurs from the surface to the Au species in all calculations and the distribution of this charge in the Au_{10} case is discussed.

1. Introduction

The discovery that small particles of Au on oxide supports are capable of CO oxidation at room temperature has excited much scientific interest recently in the catalytic,[1] surface science[2] and computational chemistry communities.[3]

A variety of oxide supports have been used in this chemistry most notably reducible oxides, such as TiO_2 and Fe_2O_3. On non-reducible supports like MgO the oxidation activity of supported Au is lower, however the use of these supports allows the study of that part of the reaction which takes place on Au and at the Au/oxide interface without the complication of the redox activity of the support. Even in this relatively simple support there is discussion as to the location of the Au particles on the surface and their charge state. Catalysts are usually prepared by deposition/precipitation from $HAuCl_4$ solution followed by calcination.[4] This results in a variety of cluster sizes whose environment on the oxide support is difficult to characterise. Landman and co-workers have used ultrahigh vacuum techniques at 90 K to deposit mass (and so size) selected Au clusters on well defined MgO(100) films.[5] By controlling the annealing temperature of the oxide film they are also able to control the number of point defects introduced. They find that the smallest Au cluster capable of catalytic activity is Au_8 and that defect rich supports give much more active catalysts compared to defect poor ones. By comparison with *ab initio* calculations they conclude that the Au particles are anchored at surface F centres resulting in negatively charged Au clusters[6] which are capable of CO oxidation.[7] In their calculations the MgO(100) surface is considered with an F_s centre formed by a five co-ordinate anion (O_{5c}) vacancy. However, recent work using scanning tunneling microscopy[8] and electron paramagnetic resonance spectroscopy[9] has suggested that point defects of this type are present in extremely low concentrations. These experiments show that extended defects such as step edges are also present on even carefully prepared MgO(100) surfaces while the concentration of point defects is vanishingly small. Electron bombardment does lead to F_s centres but these are located preferentially at edge (O_{4c} vacancy) and corner (O_{3c} vacancy) sites of steps.

Several DFT studies on Au atoms supported on MgO surfaces have appeared including direct simulations of the ultrathin MgO films grown on metallic Mo used in surface science experiments.[10,11] These indicate that adsorbed Au may actually be negatively charged due to tunneling of electrons from the metal support through the MgO film.

In this contribution we will consider the use of the SIESTA code to study Au atom and cluster adsorption on MgO surfaces. SIESTA is a local basis set code which allows relatively large system sizes to be used in modelling such structures. After showing that the results obtained are in line with earlier work we consider the adsorption of Au on extended neutral defects and show that the low co-ordinate atoms at kink sites can provide anchor points for Au clusters at least as effective as O_{5c} point defects.

In the Appendix the derivation of the pseudopotential for Au which was required as part of this work is discussed.

2. Computational details

Calculations were performed using density functional theory within the generalized-gradient approximation (GGA), using the exchange-correlation potential developed by Perdew, Burke and Ernzerhof (PBE).[12] We employ the SIESTA[13] code with its localized atomic orbital basis sets and pseudopotential representation of the core states. Development work was carried out to obtain a consistent set of pseudopotentials which included Au, details of which are given in the Appendix.

The large unit cells required in this work place some limitations on the complexity of the basis set which can be handled. We use single-ξ s, d-basis and single-p polarisation orbitals for structure optimisations (SZP) and double-ξ s, d-basis and single-p polarisation orbital for single point energy calculations (DZP). To test the reliability of the SZP

School of Chemistry, Cardiff University, Cardiff, South Glamorganshire, UK CF10 3AT. E-mail: WillockDJ@Cardiff.ac.uk

geometries the structure obtained for Au at an O_{5c} site on MgO(100) was re-optimised with the DZP basis used for all atoms in the cell. At this higher level the d(Au–O) is found to be 2.32 Å, just 0.01 Å lower than reported using our standard approach. The basis functions and the electron density are projected onto a uniform real-space grid in order to calculate the Hartree and exchange correlation potentials and matrix elements. The mesh size of the grid is controlled by an energy cutoff which sets the wavelength of the shortest plane wave that can be represented on the grid, we have taken a cutoff value of 200 Ry. In order to limit the range of the basis pseudoatomic orbitals (PAO), a common energy shift is applied, here equal to 0.01 Ry for geometry optimisations and 0.005 Ry for single point energy calculations, the basis functions are truncated at the resulting radial node. All the calculations were performed spin-polarised.

To obtain the electronic structure of the system the standard diagonalisation solution of the Hamiltonian is used in preference to the order-N, linear-scaling method. For the systems we study here (less than 250 atoms), the diagonalisation method is competitive and more convenient than the order-N method. Electronic occupations near the highest occupied state are smeared using an energy width corresponding to an effective electron temperature of 5 K. A tolerance of 10^{-4} is used for the density matrix to define when self-consistency has been achieved. For geometry optimisations the conjugate-gradient approach was used with a threshold of 0.02 eV Å^{-1}.

The MgO bulk lattice parameter has an optimized value of 4.191 Å, differing by only 0.47% from experiment (4.211 Å).[14] The optimised unit cell is used as the basis to construct all slabs used in surface calculations. The MgO(001) surface has been modelled using three-layer slabs. Previous calculations and electronic structure measurements on ultrathin MgO films have shown that the properties are well converged for three-layer films[15] and increasing the slab thickness to four MgO layers does not affect the binding energies of surface adsorbates.[11,16] For the (001) surface and the adsorption of gold atoms or gold dimers we have used 6 × 6 supercells with $a = b = 12.54$ Å, containing 108 atoms. For Au_{10} adsorption the slab dimensions were increased using 8 × 8 supercells with $a = b = 16.72$ Å containing 192 Mg/O atoms; this is sufficient to ensure that the Au_{10} adsorption energy is converged to 0.008 eV. The lower layer of the slab is fixed in all calculations involving the MgO(001) surface.

The choice of the surface to model the kink site requires more attention as a dipolar slab can arise. Periodic models containing surface kink sites can be constructed by termination at high Miller index planes. We use the MgO(1 3 10) and MgO(1 3 12) surfaces with five-layer slabs containing 200 and 250 atoms respectively. The slab geometry was chosen so that the dipole due to each kink site on one side is cancelled by an equivalent site on the other face. After relaxation of these surfaces the difference in the atomic rearrangement around the kink site in the two models is less than 0.01 Å. Using five-layer slabs, we optimise all of the layers but find that the central atoms maintain the relaxed bulk positions. The 200 atom slab is used for the single gold atom adsorption and the 250 atom slab is used for the Au_{10} gold cluster adsorption. The resulting MgO(1 3 10) supercell is orthogonal with $a = 13.22$ Å and $b = 13.86$ Å. The MgO(1 3 12) supercell is monoclinic, with $a = 13.22$ Å, $b = 17.23$ Å, $\alpha = \beta = 90°$, $\gamma = 107.87°$. All slab models employ a vacuum gap of at least 16 Å. The large real space supercells reduce the number of k-points required and only the Γ point is included for all calculations. Calculations were carried out using up to 64 processors per job on the HPCx facility.

Bader charge analysis[17] is performed using the program developed by Henkelman *et al.*[18] and XCrySDen[19] is used to display charge density isosurfaces and slices.

3. Results and discussion

Prior to adsorption of Au species the 3-layer MgO(100) surface was relaxed with the bottom layer atoms kept fixed. After relaxation the interlayer spacing increased by 0.09 Å which represents a 4% change from the bulk. Bader analysis of the calculated charge density gives 1.75 e and −1.75 e for surface Mg and O respectively, slightly less than that calculated for the relaxed bulk MgO (±1.84 e). The MgO(100) surface consists of a square network of five co-ordinate Mg^{2+} and O^{2-} ions adsorption which we refer to as Mg_{5c} and O_{5c} respectively.

In addition to the stoichiometric flat MgO(100) surface we will also consider adsorption at point and extended defects. Depending on preparation methods, it has been proposed that one of the most common surface defects on MgO(100) is the anionic vacancy; the colour or F_s centre[20] (where we use the subscript s to denote a surface colour centre). This can exist in a variety of charge states but the most widely studied is the neutral surface O vacancy, *i.e.* an F_s centre containing two electrons which are trapped by the electrostatic Madelung potential.[21] To create an F_s centre in the models presented here an O_{5c} ion is removed but the associated basis functions are left in place so that the electron density at the defect site can be described. The F_s centre formation energy calculated using our methodology is 9.06 eV and compares well with previous results using either the embedded cluster method[22] (9.07 eV) or periodic DFT calculations with plane wave basis sets and GGA functionals[23] (9.02 eV). The presence of the surface O vacancy causes very little structural relaxation even for atoms in the surface plane, reflecting the electron localization at the defect site. The surface Mg ions neighbouring the O vacancy move away from it by 0.02 Å in the surface plane while the Mg ion beneath the vacancy moves away along the surface normal by 0.06 Å. These results are in good agreement with previous studies of the MgO point defect structure.[21,24,25] Bader analysis gives an electron population for the O vacancy of 0.98 and an increase in the calculated population for the nearest substrate ions is also found.

Del Vitto *et al.* have reported work on the adsorption of gold at MgO steps[16] which contain four co-ordinate (O_{4c}) sites. However, as far as we know, no previous theoretical study has considered Au adsorption to kink sites, where O_{4c} and three co-ordinate oxygen ions (O_{3c}) are available. These defects are likely to be abundant in the materials used as catalyst supports which are usually micro-crystalline. To study the kink defect and the adsorption of single gold atoms on it, we use the MgO(1 3 10) surface (13.22 × 13.86 Å) containing 200 atoms.

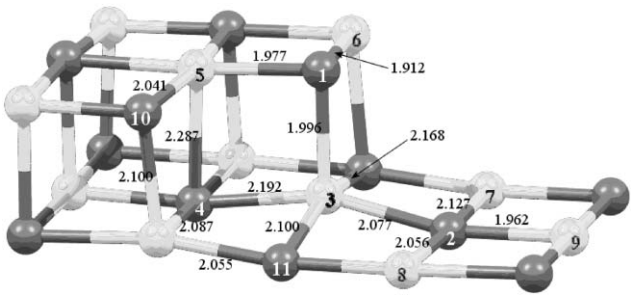

Fig. 1 Detail of the oxygen kink site on MgO(1 3 10). Bond lengths given in Å. Mg sites are shown with lighter shading than O. Only the atoms around the kink site are shown for clarity, the full formula of the simulation cell is $Mg_{100}O_{100}$.

The section of this structure around the O_{3c} kink site after relaxation is shown in Fig. 1. The step edge on this surface consists of O_{3c} kink sites (O(1)) separated by a single O_{4c} ion (*e.g.* O(10) and O(6)). The surface actually contains two step edges per unit cell, one of which presents the O_{3c} ion shown in Fig. 1 (O kink site) while the other has an Mg_{3c} ion in this position (Mg kink site). However since we will find that the interaction of Au atoms is stronger with anions we will concentrate on the kink site with three co-ordinate oxygen. The structural relaxation around these low co-ordinate species is much greater than observed for the flat MgO(100) surface or the F_s point defect. Fig. 1 gives bond lengths for the immediate vicinity of the kink site after optimisation. The calculated Mg–O bond length for bulk MgO was 2.096 Å, here the bond lengths for O_{3c} ion (O(1)) are shorter by between 0.18 and 0.12 Å. This may be expected since low co-ordination will lead to a stronger interaction between O(1) and its remaining neighbours compared to that in the bulk. It can be seen that this also influences the atomic positions of other ions in the kink region, for example, Mg(3) undergoes an upward displacement and the angle defined by O(1), Mg(5) and O(10) increases from 90° to 107.4°, probably due to anion–anion repulsion.

Bader charge analysis shows that O_{3c} has a lower electron population than found for O_{5c} on MgO(100) with a calculated charge of −1.65 *e*; this difference is balanced largely by a lower positive charge on the Mg_{4c} neighbour (Mg(6)) which had a charge of 1.70 *e*. All other surface Mg and O ions have charges within 0.03 *e* of the MgO(100) values.

3.1 Au_1 adsorption

Table 1 shows calculated data for the adsorption of atomic Au to the MgO(100) surface, the F_s centre and at the O kink site, our results are also compared to earlier calculations by Molina and Hammer,[26] Pacchioni and co-workers[11] and by Bogicevic and Jennison,[27] who applied GGA DFT with plane wave basis sets. The adsorption energy values given are calculated using the formula

$$E_{ads} = -E(\text{MgO/Au}) + E(\text{MgO}) + E(\text{Au}) \quad (1)$$

in which *E*(MgO/Au) is the total energy calculated after optimisation of the surface with the Au species present, and *E*(MgO) and *E*(Au) are the optimised energies of the clean surface and isolated Au species respectively. In each case all three calculations use the same cell dimensions and calculation parameters. Basis set superposition error (BSSE) has been taken into account in all quoted E_{ads} values using the counterpoise correction[28] unless otherwise stated. This definition implies that favourable adsorption gives a positive E_{ads} value.

For a single Au atom on defect-free MgO(100) the most favourable adsorption site is found to be directly over an O_{5c} ion, with a calculated adsorption energy around twice that for the five co-ordinate Mg site. Positioning the Au atom over the four fold hollow site formed on the square lattice of the surface results in an intermediate value for the adsorption energy. This ordering of the adsorption energy is reflected by the calculated height of the Au atom above the surface which is some 0.38 Å smaller for the O_{5c} site than for the Mg_{5c} site. Our E_{ads} values are between 0.10 and 0.15 eV lower than the PW91 values obtained by Molina and Hammer[26] and 0.13 to 0.23 eV lower than reported by Pacchioni and co-workers. Molina and Hammer also compared PW91 and RPBE functionals finding a difference of 0.31 eV in the calculated adsorption energies. Hence part of the difference between the SIESTA calculations presented here and earlier work may be due to the different functionals used and the tendency of PW91 to overestimate metal–oxide bond strengths.[11] In addition the supercell dimensions used in this work are around 10 Å larger than in the earlier papers so that Au–Au interaction effects will be minimal. Even so the relative values for the comparison of sites are in good agreement with this earlier work and all show a clear preference for Au adsorption at O_{5c} on MgO(100).

Table 1 Calculated adsorption energies and related data for Au_1 on the various surface sites of MgO

	E_{ads}/eV				Bader charge/*e*	
		PW91				
Adsorption site	This work[b]	Ref. 26	Ref. 11	*d*(Au-surf)[a]/Å	Au	Ads. site
O_{5c}/MgO(100)	0.78 (1.13)	0.88	1.01	2.33	−0.31	−1.47
Mg_{5c}/MgO(100)	0.36 (0.67)	0.51	0.49	2.71	−0.21	1.74
Hollow/MgO(100)	0.61 (0.92)	0.72	—	2.41	−0.27	—
F_s/MgO(100)	2.83 (3.25)	3.17[c]	—	1.88	−1.12	−0.38
O kink/MgO(1 3 10)	1.08 (1.54)	—	—	2.17	−0.28	−1.38[d]

[a] For MgO(100) *d*(Au–surf) is the height of the Au atom above the surface, for the O kink site the smallest Au–O distance is given. [b] Values in parentheses are prior to BSSE correction. [c] Value taken from PW91 data in reference 27. [d] Value calculated for O(1) in Fig. 4.

The outer electronic structure of Au is $4f^{14}5d^{10}6s^1$, with the 5d and 6s levels expected to be important in bonding. The 6s shell relativistic contraction is more pronounced in Au than for any other element in the same row of the periodic table,[29] an effect which gives gold a higher electron affinity than other elements in the same group (2.31 eV *cf.* 1.30 eV for Ag and 1.23 eV for Cu). The calculated Bader charges in Table 1 all show negative Au species indicating that charge transfer from the surface to the Au atoms has taken place. For the single Au atom adsorbed over the O_{5c} site we see a decrease in the magnitude of charge on the co-ordinating O^{2-} ion by 0.28*e* compared to the clean surface. For adsorption at the Mg site the calculated Bader charge on Mg_{5c} is practically unaltered compared to the clean surface despite a significant charge transfer to the Au atom. This effect can be understood from the partial density of states calculated from the band structure of the slab with Au adsorbed on the O_{5c} site which is shown in Fig. 2. The highest occupied band for the MgO system is O 2p in character and the presence of the Au adsorbate introduces a gap state around 1 eV above the top of the occupied states for the MgO slab. The Fermi level falls within this feature signifying that the states localised at Au are partially occupied. This feature is formed mainly from a combination of the Au 6s and O 2p states with the Au 5d states making a small contribution. The interaction that this represents is responsible for the observed charge transfer from the surface to the adsorbate. The Au 5d states make a more significant contribution to filled states close in energy to the top of the MgO valence band.

To study the charge transfer between Au and the MgO surface further we make use of the charge density difference

$$\rho_{\text{diff}} = \rho(\text{Au/MgO}) - \rho(\text{Au}) - \rho(\text{MgO}) \qquad (2)$$

which is the difference between the charge density of the Au/MgO system and that for Au and MgO in isolation. ρ_{diff} Is positive in the regions where there is a gain of electronic charge upon formation of the complete system, and negative where there is a loss of electronic charge. Fig. 3*a* shows loss of electron density for both the surface O^{2-} ion and the Au adsorbate along the surface normal direction. For the Au atom the region of charge increase is much more diffuse and in this cross-section can only be seen in the two regions to the side of the atomic centre. Loss of charge in the region between the Au atom and surface O^{2-} ion argues against a covalent interaction between the two atoms. However the asymmetry in the regions showing charge depletion around the Au centre suggests that it has become polarised to give a favourable interaction with the surface, in agreement with planewave DFT results.[16] The pattern of the difference density also shows that charge transfer has occurred both from the surface to the diffuse Au 6s state and from the Au 5d levels into the Au 6s. The interaction has a very local nature, since charge density difference is only significant in the immediate region of the O_{5c} adsorption site, confirming that the states observed at the Fermi level in Fig. 2 should be regarded as localised surface states.

Of the alternatives covered here the adsorption of a single gold atom at the F_s vacancy site is considerably more favourable than any of the sites on stoichiometric surfaces giving a value for E_{ads} 1.75 eV higher than the O kink site. The adsorption energy is, again, smaller than the literature planewave PW91 value, in line with the results from the non-defective MgO(100) surface. The Au atom sits much closer to the surface than for any of the earlier MgO(100) sites, at 1.88 Å the interfacial distance, *i.e.* the perpendicular distance between Au and the top layer of the surface, is 0.45 Å shorter than was found for the O_{5c} site. This positioning agrees well with published results for Ag on an MgO(100) F_s centre, for which Zhukovskii and Kotomin[30] reported an interfacial distance of 1.81 Å and Matveev *et al.*[31] found 1.84 Å.

Adsorption of Au at the F_s centre also leads to a charge transfer from the defect to the Au atom. The Bader charge on the gold atom is found to be −1.12 *e* so that it has gained 0.81 electrons more than in the case of the perfect surface with Au at the O_{5c} site. The charge at the vacancy site is −0.38 *e*,

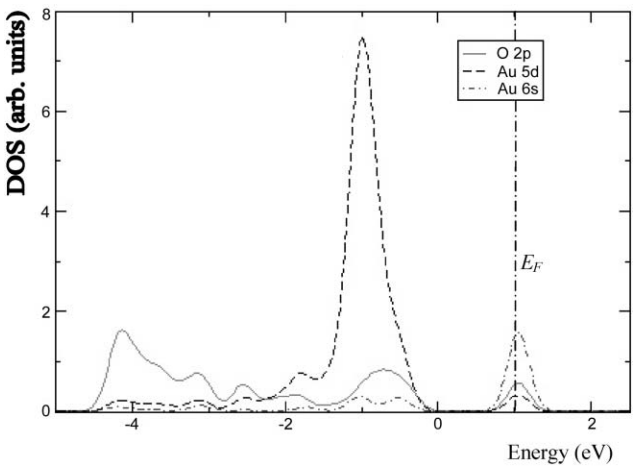

Fig. 2 Projected density of states showing the Au 6s, 5d and O 2p states for Au adsorbed on O_{5c} of the MgO(100) surface. A Gaussian smearing width of 0.2 eV is applied. The energy origin is chosen as the top of the 2p valence band for the surface oxygen anions not directly interacting with Au.

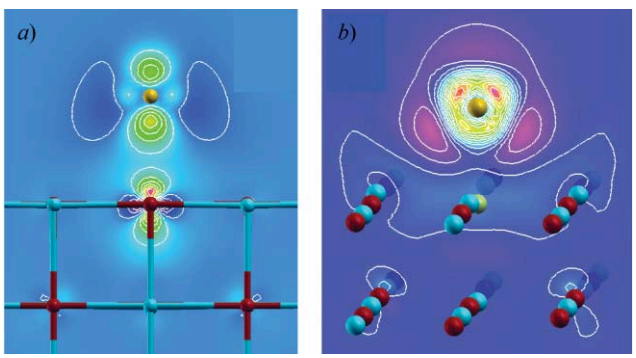

Fig. 3 Charge density difference for *a*) Au_1 adsorbed onto a five co-ordinated oxygen atom of the MgO(100) surface and *b*) Au_1 adsorbed at an F_s centre defect site. Red/green colours represent charge depletion and blue/purple colours charge accumulation. Lines are drawn in intervals of *a*) 0.01 $e\ a_0^{-3}$ and *b*) 0.002 $e\ a_0^{-3}$. Atoms coloured: O: red, Mg: blue, Au: yellow, a green marker is also placed in the defect and used as the centre for the associated basis functions.

less than half of the value found prior to Au adsorption. Zhukovskii and Kotomin[30] report that for the adsorption of Ag or Cu over an F_s centre a charge of about -0.5 e is transferred from the surface defect to the metal atom. The charge density difference in Fig. 3*b* shows an accumulation of charge around the gold atom and suggests that the electron density has been transferred from the vacancy to the Au 6s level in a similar manner to the Au on the O_{5c} site shown in Fig. 3*a*. However in this case the charge accumulation can also be seen more clearly in the region between the Au atom and surface Mg^{2+} sites neighbouring the defect. These results indicate that adsorption of a Au atom at an oxygen vacancy is accompanied by an electron transfer from the defect site to the Au centre which is then polarised to give favourable interactions with the cations surrounding the defect.

The MgO(100) results have suggested that the strongest interaction of a Au atom with a stoichiometric surface will be through the O_{5c} sites. In an extended defect such as a step edge or kink site we reasoned that it may be possible to enhance the adsorption energy through multiple Au···anion interactions and so Au adsorption at the O kink site on MgO(1 3 10) was also considered. Three different starting geometries were chosen, using the numbering scheme defined in Fig. 1 these were:

i) Au along side $O_{3c}(1)$ and over $O_{5c}(2)$, this structure relaxed to give the geometry shown in Fig. 4 with an E_{ads} value of 1.54 eV before BSSE correction.

ii) The Au atom was placed at equal distances from $O_{3c}(1)$, $O_{4c}(10)$ and $O_{5c}(11)$. This configuration was expected to give the highest adsorption energy as gold is in contact with three oxygen ions. However, during the optimisation the gold atom moved out of the kink to give a geometry similar to Fig. 4 and so the same minimum was obtained as from starting point (i).

iii) Au on top of $O_{3c}(1)$, this starting point relaxed to give a Au–$O_{3c}(1)$ distance of 2.21 Å and adsorption energy of 1.44 eV without BSSE correction.

Adsorption on an O_{5c} anion in the terrace area of the MgO(1 3 10) surface was also tested but results were very similar to the adsorption of Au on the oxygen site of the regular MgO(100) surface. Accordingly, the structure shown in Fig. 4 corresponds to the most stable adsorption state of Au at the kink site of MgO(1 3 10) and the BSSE corrected adsorption energy for this structure is quoted in Table 1. At the O kink site the Au distance to $O_{3c}(1)$ is 2.17 Å while the distance to the next nearest O neighbour, $O_{5c}(2)$, is 0.51 Å further, at 2.68 Å which is also longer than the Au–O distance at the O_{5c} site on MgO(100). The Mg···$O_{3c}(1)$ nearest neighbour distances are also longer with the Au adsorbate present than in the relaxed surface structure shown in Fig. 1, most notably the Mg(5)···$O_{3c}(1)$ distance opposite to the Au adsorbate and the Mg(3)···$O_{3c}(1)$ distance. Bader charge analysis shows that $O_{3c}(1)$ now has a charge of -1.38 e, representing a loss of 0.27 electrons after gold adsorption. The charge on the gold atom is -0.28 e, and so it appears that only $O_{3c}(1)$ is really participating in the charge transfer between the surface and the Au atom. The charge density difference plot shown in Fig. 5 also shows charge depletion from $O_{3c}(1)$ with only minor changes to the charge density around $O_{5c}(2)$. So it appears that even in this environment with the possibility of high co-ordination for the Au atom charge transfer and polarisation occurs only *via* a single atom–atom interaction. The higher adsorption energy for the Au atom at the step arises through interaction with a low co-ordination surface anion rather than through multiple Au–anion interactions.

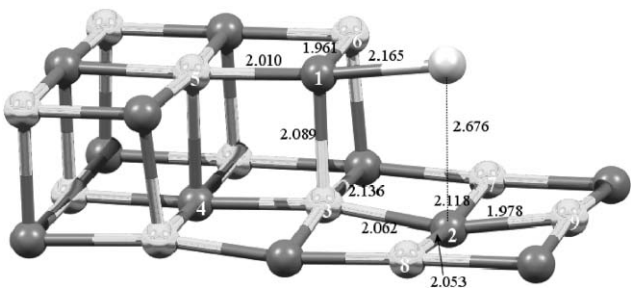

Fig. 4 Optimised structure for Au adsorbed at the oxygen kink site of the MgO(1 3 10) surface. Selected distances are given in Å. Atoms shaded: O dark, Mg and Au light, Au is bonded to O(1).

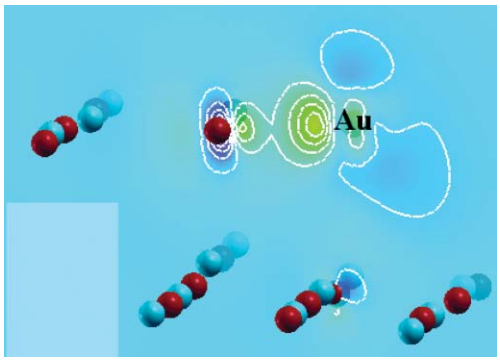

Fig. 5 Charge density difference for a single gold atom adsorbed at the oxygen kink site of the MgO(1 3 10) surface. Red/green colours represent charge depletion and blue/purple colours charge accumulation. Lines are drawn in intervals of 0.01 e a_0^{-3}. Atoms coloured: O: red, Mg: blue, Au: yellow.

Studying gold adsorption at steps on an MgO surface, Del Vitto *et al.*[16] found a similar configuration for the most stable adsorption site, with the gold atom much closer to the O_{4c} of the step than the O_{5c} of the lower plane. We obtain an adsorption energy of 1.08 eV (Table 1) which is 28% higher than on the terrace. Del Vitto *et al.* reported a binding energy of 1.26 eV at the MgO step using PW91 functionals, 40% higher than on their terrace site.

3.2 Au_2 adsorption

The growth of a Au cluster from the initial adsorption of a single Au atom would be expected to pass through a dimer stage. This is the smallest cluster we can use to consider the effect of the geometry of the Au species and its arrangement with respect to the surface. The calculated adsorption energies and geometric parameters for a Au dimer on the MgO(100) and F_s centre are summarised in Table 2. Since the results with a single Au atom point to a strong preference for the O_{5c} site on the MgO(100) surface we used this as the starting point for Au_2 adsorption. Minima were obtained with the dimer axis

Table 2 Adsorption energies and geometrical parameters for Au_2 on the MgO(100) surface and at an F_s defect site

Adsorption site	E_{ads}/eV		Au(1)–surf[b]/Å	Au(1)–Au(2)/Å	Tilt angle[c] θ/°
	This work[a]	PW91, ref. 26			
MgO(100)/Au_2(perp.)	1.27 (1.61)	1.36	2.19	2.56	0
MgO(100)/Au_2(parallel)	0.54 (1.11)	—	2.52	2.63	90
F_s Vertical	3.38 (3.86)	3.89	1.69	2.62	0
F_s Mg-tilted	3.49 (4.12)	4.17	1.68	2.74	59
F_s O-tilted	3.33 (4.00)	3.91	1.66	2.72	61

[a] Values in parentheses are prior to BSSE correction. [b] Au(1)–surf is the perpendicular distance of Au(1) from the top layer of the surface. [c] Angle between Au_2 axis and surface normal as defined in Fig. 6.

either parallel or perpendicular to the surface plane. The calculated adsorption energies suggest a strong preference for the perpendicular arrangement which has an E_{ads} value 0.73 eV higher than the parallel. The perpendicular arrangement E_{ads} value is also 0.49 eV higher than that for a single Au atom adsorbed to the same site. This relative stability can be understood in terms of the polarisation of the adsorbed species. A Bader analysis of the perpendicular dimer gives a charge on the Au atom closest to the O_{5c} site (Au(1)) of -0.07 *e* whereas the other Au atom has a calculated charge of -0.25 *e*. The total charge transfer from the surface to the adsorbed species is similar to that for the single Au atom, however the charge is distributed in the dimer to be away from the surface anion. The second Au atom above the first effectively enhances the polarisability of the adsorbate and allows the charge to be shifted further from the surface reducing unfavourable electrostatic interactions.

The gold dimer adsorbed horizontally relaxes to a structure in which the Au atoms interact with two surface O_{5c} ions with the molecular axis arranged diagonally across a hollow site. The resulting dimer bond length is 2.63 Å and the adsorption energy is 0.24 eV less favourable than that for the adsorption of a single gold atom at an O_{5c} site. In this parallel arrangement both Au atoms have the same Bader charge (-0.18 *e*) and so the enhanced polarisability observed in the perpendicular arrangement is not present. The relatively large atomic radius of Au also prevents Au_2 adsorption parallel to a surface Mg–O neighbour pair, which may be expected to lead to strong polarisation of the dimer. Molina and Hammer have pointed out that this difference between the parallel and perpendicular adsorption modes for Au_2 on the defect free MgO(100) surface would favour 3-D growth of Au particles rather than 2-D monatomic film formation.[26]

As was found for the Au_1 case, adsorption of Au_2 at an F_s centre is considerably more favourable than for the defect free surface. Three local minima exist for the dimer adsorbed at the vacancy site. The most stable configuration, "Mg-tilted", has one Au atom directly on top of the vacancy and the other interacting with a neighbouring magnesium ion; atoms 1 and 2 respectively as shown in Fig. 6. This structure is around 0.27 eV lower in energy than the two other minima which correspond to a tilting toward O and the dimer perpendicular to the surface. Using the GGA PW91 functional with VASP, Del Vitto *et al.*[16] obtain an energy difference of 2.68 eV between the vertical dimer on the defect free MgO(100) surface and the Mg-tilted geometry on the F_s centre. Although the absolute values of our adsorption energies in Table 2 are lower than this earlier work the energetic ordering of the alternative structures is the same.

Fig. 6 defines the tilt angle with respect to the surface normal and for both Mg-tilted and O-tilted structures an angle of around 60° is found, which places Au(2) 3.13 Å from the surface O^{2-} ion in the O-tilted structure and 2.80 Å from the surface Mg^{2+} ion in the Mg-tilted structure. The apparent closer approach to the surface of Au(2) in the latter case is mainly due to the movement of the surface Mg^{2+} ion toward the Au atom as can be seen in Fig. 6. This Mg ion moves 0.33 Å from its initial position toward Au(2) during the optimisation process while the corresponding O ion in the O-tilted configuration moves away from Au(2) by 0.09 Å.

At the F_s centre the charge transferred to the dimer is distributed between the two Au atoms. For example for the Mg-tilted geometry we find Bader charges of -1.06 *e* and -0.59 *e* for Au(1) and Au(2) respectively. This represents a total charge transfer from the defect to the Au species greater in magnitude than found for the single Au atom at the F_s centre by 0.53 *e*. The Bader analysis now gives zero charge at the vacancy site. Charge density difference maps (not shown) indicate a similar charge decrease in the region between Au(1) and the defect site as found for the Au atom but this is now accompanied by accumulation of electron charge between both Au(1) and an Mg^{2+} ion neighbouring the defect and between Au(2) and the Mg^{2+} ion that has moved out of the surface.

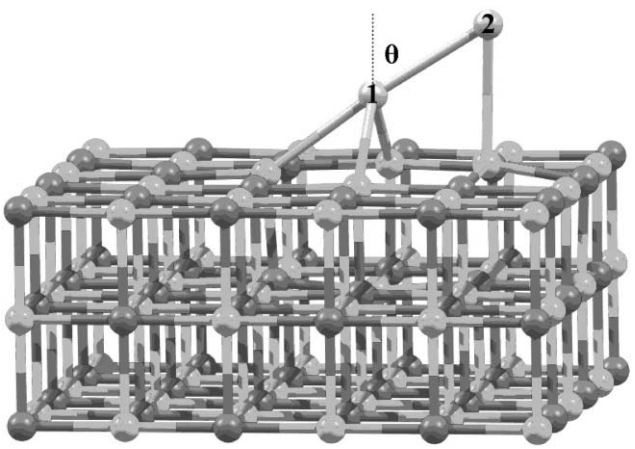

Fig. 6 Geometry of the gold dimer adsorbed at the F_s centre of MgO(100) and orientated with Au(2) on top of Mg_{4c}. θ is the angle formed by the Au_2 axis and the normal to the plane. Atoms shaded: O: dark, Mg and Au: light.

3.3 Au_{10} adsorption

Using an empirical many-body potential, Wilson and Johnston[32] found a bicapped square anti-prism structure with D_{4d} symmetry as the global minima for Au_{10} in the gas phase. Rogan *et al.* found the same optimal geometry for Au_{10}, using both DFT with the PBE functional and classical molecular dynamics in combination with embedded atom potentials.[33] However on the MgO(100) surface our calculations showed that this geometry tends to flatten and so we also chose a geometry based on two layers from the bulk fcc structure for Au_{10} with a (7,3) structure. This structure has also been used to model Au_{10} on $TiO_2(110)$[34] and is consistent with STM images of Au clusters formed on FeO(111).[35] The optimised geometry for this cluster on the MgO(100) surface is shown in Fig. 7.

The distance between the surface and the bottom layer of the cluster is on average 2.67 Å. This cluster–surface distance lies within the range previously calculated for single Au atom adsorption, 2.33–2.71 Å (Table 1), gold atom 7 at the centre of the cluster in Fig. 7 is 2.49 Å above a surface oxygen ion, further than either the single gold atom (2.33 Å) or the perpendicular dimer (2.19 Å). The optimised interlayer spacing within the Au cluster is 2.19 Å compared to the optimised bulk value of 2.36 Å.

To calculate the adsorption energy of the cluster we again use eqn (1) but the reference state for the Au_{10} cluster (E(Au)) has been taken from the reference calculation on the bulk structure of Au discussed in the Appendix. This reference state is more satisfactory than the gas phase cluster since it is the energy required to remove the 10 atoms from the bulk Au structure and place them as a cluster on the surface, so that a positive value implies that it is more stable for the cluster to adhere to the surface than for clusters to segregate into larger particles. For the Au_{10}(7,3) structure on MgO(100) we calculate an adsorption energy of 24.7 eV using this reference state.

Bader charges calculated for the Au_{10} cluster in the Au_{10}/MgO(100) model are given in Table 3. The cluster has a total charge of -0.88 e with the largest contribution to this from the lower layer of the cluster, especially atoms 2 and 5 (Fig. 7) which contribute almost 70% of the total charge. These two gold atoms are situated at opposite sides of the cluster separated by a distance of 6.3 Å. The central atom, Au(7), which is directly over a surface oxygen ion has a small positive charge and so the Bader analysis suggests a re-distribution of charge to the periphery of the lower layer of the cluster. Atoms 8, 9 and 10 representing the top of the cluster are almost neutral so comparing this distribution with our results for the perpendicular dimer adsorption suggests that larger clusters distribute donated charge amongst the lower layers rather than polarising perpendicular to the surface.

Table 3 Bader charges for Au_{10}/MgO(100), for atom labels refer to Fig. 7

Au atom[a]	Charge/e	Au atom[a]	Charge/e
1	−0.05	6	−0.03
2	−0.29	7	0.09
3	−0.10	8	0.01
4	−0.11	9	−0.04
5	−0.32	10	−0.04

[a] Atoms numbered according to Fig. 7.

The F_s centre represents an anchorage point for Au_{10} and the bi-capped anti-prism structure retains its gas phase structure on adsorption at this site, as shown in Fig. 8. Two orientations are possible for this structure; atoms of the second layer (Au(2) to Au(5) in Fig. 8) can either lie above O^{2-} or Mg^{2+} ions neighbouring the defect centre. The adsorption energy is 26.7 eV for the "on top of Mg" orientation and 25.0 eV for the "on top of O" orientation. As expected from the tilted dimer calculations at the F_s site the arrangement with the secondary atoms over the cation sites is favoured. In this structure atom Au(1) is 1.54 Å above the F_s centre, which is smaller than the interfacial distance for a single Au atom (1.88 Å) or for the dimer (1.68 Å). Bader charge analysis of the Au_{10} cluster in this bi-capped anti-prism geometry at the F_s centre is reported in Table 4. The Bader charge of the F_s centre is now zero, as was found for the Mg-tilted dimer structure. Atom Au(1), directly on the top of the F_s centre, has a charge of -1.06 e, equal to that of the Au(1) atom in the dimer. The rest of the cluster charge is mainly distributed over the layer 2

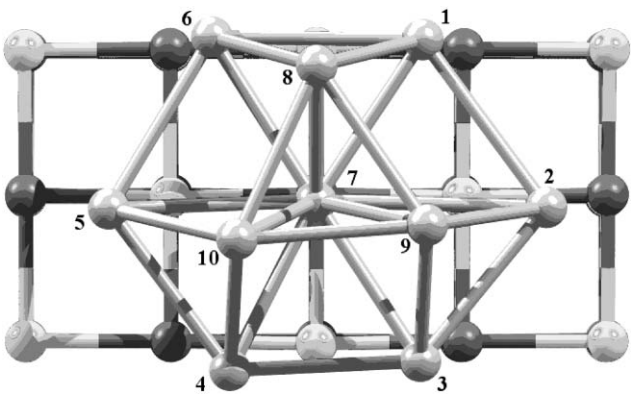

Fig. 7 Top view of the Au_{10} cluster adsorbed onto the MgO(100) surface showing numbering of the gold atoms. Only a section of the surface is shown for clarity; the full formula of the 3 layer MgO simulation slab was $Mg_{54}O_{54}$. Atoms shaded: O: dark, Mg and Au: light, with Au atoms numbered.

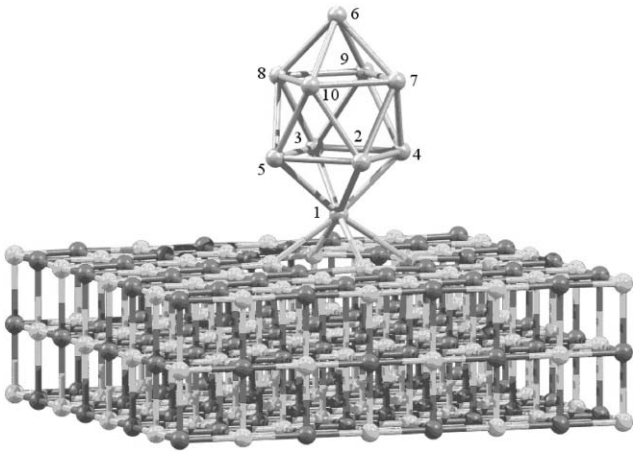

Fig. 8 Geometry of the bi-capped anti-prism Au_{10} cluster adsorbed on the F_s centre. Atoms shaded: O: dark, Mg and Au: light, with Au atoms numbered.

Table 4 Calculated Bader charges for the Au_{10} cluster adsorbed in its bi-capped anti-prism geometry on the F_s centre, for atom labels refer to Fig. 8

Layer[a]	Au atom[b]	Charge/*e*	Layer[a]	Au atom[b]	Charge/*e*
1	1	−1.060	3	7	−0.029
2	2	−0.085		8	−0.050
	3	−0.112		9	−0.032
	4	−0.126		10	−0.042
	5	−0.129	4	6	−0.040

[a] Layer 1 is the single Au atom closest to the defect site. [b] Atoms numbered according to Fig. 8.

gold atoms, Au(2) to Au(5), which are over Mg^{2+} cations. The other Au atoms have small negative charges similar to the second layer atoms in the Au_{10}(7,3) structure on the perfect MgO(100) surface. The total charge of the cluster (−1.71 *e*) is very close to the total charge found for the dimer (−1.65 *e*), suggesting that the amount of charge transferred from the F_s to the gold clusters has reached a limit at $\sim$−1.7 *e* which is in good agreement with formal charge analysis since the F_s centre is expected to contain only two electrons.

We have also considered the adsorption of the Au_{10}(7,3) structure on the F_s centre and the optimised geometry is shown in Fig. 9. The adsorption energy of this species is 27.5 eV, 0.8 eV greater than that for the bi-capped anti-prism. In addition the geometry of the Au_{10}(7,3) structure alters significantly on optimisation. Although in this structure the two layers are still distinct the lower layer atoms have been moved away from their initial positions so that Au(1)–Au(6) all have nearest neighbour surface atoms that are O^{2-} ions. One effect of the lower layer re-arrangement on optimisation is that the distance between Au(1) and Au(6) is much greater than in the isolated cluster or in the cluster adsorbed to the MgO(100) surface and Au(8) in the second layer is closer to the surface than Au(9) or Au(10). It has been pointed out by Molina and Hammer[26] that the distance between the anions on the MgO(100) surfaces matches closely with the Au(100) surface of the bulk. This may be expected to cause the disruption to this relatively small cluster in which the Au atoms are

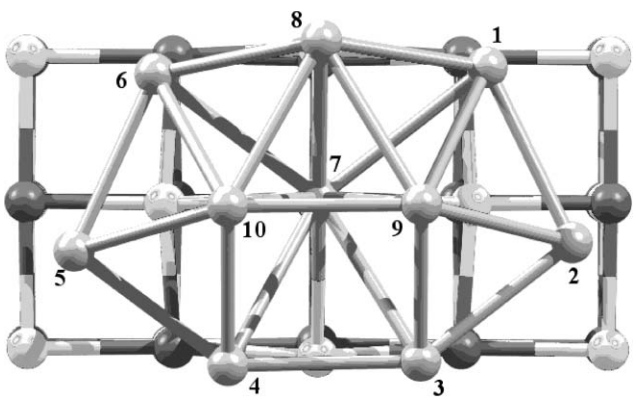

Fig. 9 Top view of the Au_{10}(7,3) cluster adsorbed on the F_s centre showing the numbering of the gold atoms used in the text. Only a section of the surface is shown for clarity, the full formula of the 3 layer MgO simulation slab was $Mg_{54}O_{53}$. Atoms shaded: O: dark, Mg and Au: light.

Table 5 Calculated Bader charges for the Au_{10}(7,3) cluster on an F_s centre, for atom labels refer to Fig. 9

Au atom[a]	Charge/*e*	Au atom[a]	Charge/*e*
1	−0.206	6	−0.182
2	−0.244	7	−0.947
3	−0.155	8	−0.061
4	−0.118	9	−0.007
5	−0.251	10	−0.023

[a] Atoms numbered according to Fig. 9.

initially more tightly packed in a Au(111) surface array. However relatively minor changes were seen for the MgO(100) case and so this is not the only factor in the change of structure for the Au_{10}(7,3) cluster at the F_s centre.

The Bader charge for the F_s centre is again zero but now the total charge of the cluster is −2.19 *e*. This represents a gain of 0.49 electrons compared to the upper limit we have set for electron transfer from the defect itself based on Au_2 and the bi-capped anti-prism Au_{10} cluster at the F_s centre. This implies that charge transfer occurs not only from the F_s centre but also from the surface anions with which the cluster interacts. Table 5 shows that the charge is concentrated on the lower layer atoms as was found for the Au_{10}(7,3) cluster on the perfect surface. At the defect, however, Au(7) directly over the F_s site now carries a large negative charge and the average charge on the other lower layer Au atoms is greater in magnitude than in the previous case. This charging of the lower layer of the cluster would be expected to produce repulsive electrostatic forces between the Au atoms that will also contribute to the geometry changes observed on optimisation.

For the Au_{10} cluster adsorption at an O kink site we use the MgO(1 3 12) surface to increase the surface area of the simulation cell compared to the MgO(1 3 10) structure used for Au_1. The structures of the kink sites on these surfaces are the same but the terrace region is larger on MgO(1 3 12) than on MgO(1 3 10). The initial geometry of the cluster was taken as its gas phase optimal geometry (bi-capped anti-prism), placed with one of the triangular faces of the anti-prism on the terrace and a capping atom close to the O kink site. During optimisation the shape of the cluster gradually changes to adopt a Au(7,3) like geometry as shown in Fig. 10. The binding energy calculated for this structure is considerably greater than for the alternative Au_{10} structures considered at 34.6 eV. The closest point of contact for this structure with the surface is at the O_{3c} site which was also found to be involved in the charge transfer to a single Au atom adsorbate. There are also two close Au–O_{4c} interactions and one Au–O_{5c}. In addition, even on the MgO(1 3 12) surface, the cluster is able to bridge the terrace and an interaction with the Mg_{3c} of the second kink site in the simulation cell is clearly visible. Indeed this Mg_{3c} atom moves out of the surface and is closer to a Au atom of the cluster than the oxygen anion that was below it in the relaxed clean surface. Unfortunately the charge density difference and Bader analysis are currently limited to orthorhombic cells and so it was not possible to consider the charge distribution for the MgO(1 3 12) system in the same detail as earlier structures. However the interaction of the cluster with both surface anions

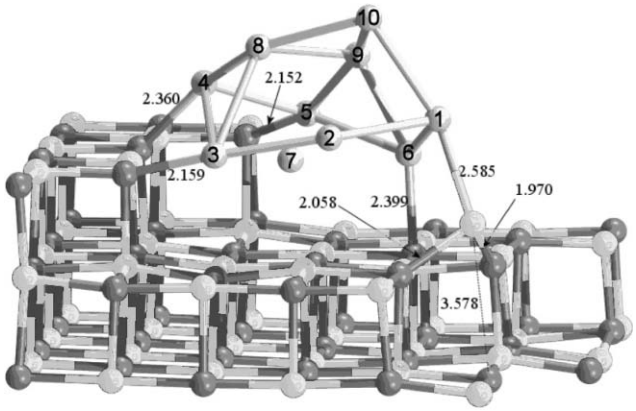

Fig. 10 Au_{10} cluster adsorbed at the oxygen kink site of the MgO(1 3 12) surface. Only a section of the surface is shown for clarity, the full formula of the 3 layer MgO simulation slab was $Mg_{125}O_{125}$. Selected distances are given in Å. Atoms shaded: O : dark, Mg and Au: light.

and cations suggest a similar model of negative charge transfer and charge redistribution within the cluster as has been seen for earlier models.

4. Conclusions

We have demonstrated that the efficient coding of the SIESTA package coupled with the power of national facilities such as HPCx enable periodic DFT to be applied to consider the adsorption of metal particles to oxide interfaces.

In our specific example of Au on MgO adsorption at the thermodynamically most stable surface, MgO(100), is relatively weak compared to point and kink defect sites. For single Au atoms and dimers adsorption at F_s point defects gives adsorption energies more than twice those for the flat stoichiometric surface. This is in agreement with earlier work that suggested that point defects may be required to anchor Au clusters on MgO surfaces. However for Au_{10} we also find that higher index surfaces with kink sites present can have cluster adsorption energies higher than the F_s centre point defect on MgO(100). At the F_s centre charge transfer occurs mainly to the Au atom directly over the defect with some delocalisation to the lower layer atoms of the cluster. An Au_{10} cluster on the MgO(1 3 12) is able to set up multiple interactions with low co-ordination ions leading to the greater calculated interaction energy. This suggests that catalyst supports with extended defects offering low co-ordination surface sites will be able to maintain Au particle dispersion without the need for F_s centres.

All the structures studied here formally contain Au atoms in the zero oxidation state. Charge transfer from the surface leads to negatively charged atoms, dimers and clusters and interaction with the F_s centre giving species close to Au^-. For Au_2 and Au_{10} the charge is redistributed through the cluster leading to favourable $Au^{\delta-}\cdots Mg^{2+}$ interactions. In the Au_{10} cluster this redistribution involves mainly atoms in the lower layers for both the bi-capped anti-prism and $Au_{10}(7,3)$ structures. The effect of the negative charge on catalysis would therefore be expected to be confined to reactions occurring at the metal oxide interface.

The models presented here do not contain species that may be expected to oxidise Au on the surfaces studied. The presence of Au^0 and oxidised Au species together has recently been shown to be optimal for the CO oxidation reaction[36] and so Au^+ and Au^{3+} species are the subject of our current research.

Appendix

The techniques used to derive pseudopotentials for this work were largely based on the approach of Giannozzi and co-workers.[37] The SIESTA pseudopotentials (PP) are generated using the program ATOM which is supplied as part of the program suite. To be consistent with the work described in the main text PP generation calculations employed the PBE functional.[12] We employ the widely used scalar relativistic Troullier–Martins pseudopotentials[38] with nonlinear core corrections[39] in their fully non-local form.[40] These were generated with the reference configurations $6s^1\ 6p^0\ 5d^{10}$ for Au, $3s^2\ 3p^0\ 3d^0$ for Mg, $2s^2\ 2p^4\ 3d^0$ for O, $2s^2\ 2p^2\ 3d^0$ for C and $1s^1\ 2p^0\ 3d^0$ for H. The cutoff radii for the s, p and d components of the pseudopotentials are 2.40, 2.70 and 1.90 a.u. for Au; 1.90 and 2.30 a.u. for Mg; 1.30 a.u. for O, 1.40 a.u. for C and 0.80 a.u. for H. The match to all electron calculations for the case of Au is shown in Fig. 11.

Relativistic effects are taken into account for Au and a nonlinear core correction is applied for Au and Mg, with r_{pc} = 1.20 a.u. for both, so that the pseudocore charge density equals the charge density outside r_{pc}, this has the smooth form $\rho_{pc} = Ar\sin(br)$ inside that radius and is continuous up to second derivatives at r_{pc}. Furthermore, semi-core $2p^6$ electrons are explicitly treated for Mg when single point energy calculations are performed for Bader analysis.

Transferability

To test transferability of the pseudopotential for Au we tested the results of PP and AE atomic calculations on atomic configurations differing from the one used in the fitting procedure. We chose three different atomic configurations: $[5d^{10}\ 6s^1]$, $[5d^9\ 6s^2]$ and $[5d^{10}\ 6s^0\ 6p^1]$ corresponding respectively to the ground state, an excited state with promotion of a 5d electron to the 6s orbital and an excited state with promotion of a 6s electron to the 6p orbital. The calculated estimates of the excitation energies differed between the AE and PP methods by at most 3.7 mRy for excitations involving the ground state and by 3.4 mRy for the first and second excited states.

In addition to these reference state calculations for atomic Au we have also tested the ability of calculations using the new pseudopotential to reproduce reference data on bulk Au and the gas phase Au_2 dimer. Our results are compared to the earlier study of Soler *et al.*[41] and experimental reference data in Table 6. The gold bulk lattice parameter has an optimised value of 4.088 Å, only 0.22% greater than the experimental value (4.079 Å).[42] Soler *et al.*, also using SIESTA but with LDA, quote a very similar value (4.069 Å) which is below experiment as LDA tends to result in over-binding. The gold dimer bond length r_e at equilibrium obtained here (2.483 Å) differs from the experimental value (2.472 Å)[45] by only 0.44%. Using the CCSD(T)[43] level of theory, Varganov *et al.*[44]

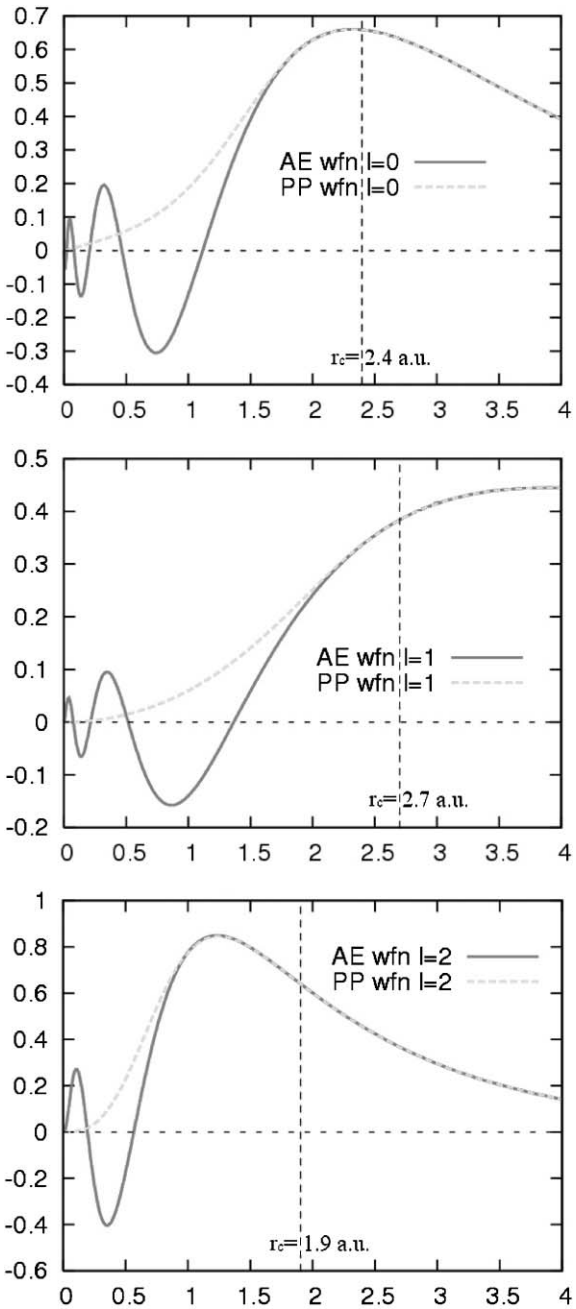

Fig. 11 All-electron (AE) and pseudopotential (PP) wave functions for Au at *a*) $l = 0$, *b*) $l = 1$ and *c*) $l = 2$. r_c is the radius cutoff in a.u.

Table 6 Lattice parameter of bulk gold Au(s) and bond length of Au_2 dimer

	This work	Soler *et al.*[41]	Expt.
Au(s), *a*/Å	4.088	4.069	4.079
Au_2, r_e/Å	2.483	2.460	2.472

calculated a bond length of 2.535 Å for Au_2, which differs by 2.55% from the experimental value[45] of 2.472 Å even though this method provides a better estimate of dynamic correlation than does DFT. We also tested the gold pseudopotential with Au^+ using AuH. A bond length d(Au–H) = 1.564 Å was calculated, *vs.* 1.524 Å obtained experimentally.[46]

Acknowledgements

We would like to thank the Materials Consortium for provision of time on HPCx and SASOL for an industrially sponsored studentship.

References

1 M. Haruta, *CATTECH*, 2002, **6**, 102.
2 R. Meyer, C. Lemire, Sh. K. Shaikhutdinov and H.-J. Freund, *Gold Bull.*, 2004, **37**, 72.
3 L. M. Molina, M. D. Rasmussen and B. Hammer, *J. Chem. Phys.*, 2004, **120**, 7673.
4 M. Haruta, *Catal. Today*, 1997, **36**, 153.
5 A. Sanchez, S. Abbet, U. Heiz, W.-D. Schneider, H. Häkkinen, R. N. Barnett and U. Landman, *J. Phys. Chem. A*, 1999, **103**, 9573.
6 B. Yoon, H. Häkkinen, U. Landman, A. S. Wörz, J.-M. Antonietti, S. Abbet, K. Judai and U. Heiz, *Science*, 2005, **307**, 403.
7 L. D. Socaciu, J. Hagan, T. M. Bernhardt, L. Wöste, U. Heiz, H. Häkkinen and U. Landman, *J. Am. Chem. Soc.*, 2003, **125**, 10437.
8 M. Sterrer, M. Heyde, M. Novicki, N. Nilius, T. Risse, H-P. Rust, G. Pacchioni and H-J. Freund, *J. Phys. Chem. B*, 2006, **110**, 46.
9 M. Sterrer, E. Fischbach, T. Risse and H-J. Freund, *Phys. Rev. Lett.*, 2005, **94**, 186101.
10 G. Pacchioni, L. Giordano and M. Baistrocchi, *Phys. Rev. Lett.*, 2005, **94**, 226104.
11 L. Giordano, M. Baistrocchi and G. Pacchioni, *Phys. Rev.*, 2005, **72**, 115403.
12 J. P. Perdew, K. Burke and M. Ernzerhof, *Phys. Rev. Lett.*, 1996, **77**, 3865.
13 J. M. Soler, E. Artacho, J. D. Gale, A. García, J. Junquera, P. Ordejón and D. Sánchez-Portal, *J. Phys.: Condens. Matter*, 2002, **14**, 2745.
14 D. Taylor, *Br. Ceram. Trans. J.*, 1984, **83**, 5.
15 S. Schinkte, S. Messerli, M. Pivetta, F. Patthey, L. Libioulle, M. Stengel, A. Del Vita and W.-D. Schneider, *Phys. Rev. Lett.*, 2001, **87**, 276801.
16 A. Del Vitto, G. Pacchioni, F. Delbecq and P. Sautet, *J. Phys. Chem. B*, 2005, **190**, 8040.
17 R. Bader, *Atoms in Molecules: A Quantum Theory*, Oxford University Press, New York, 1990.
18 G. Henkelman, A. Arnaldsson and H. Jónsson, *Comput. Mater. Sci.*, 2006, in press.
19 A. Kokalj, *J. Mol. Graphics Modell.*, 1999, **17**, 176.
20 U. Heiz and E. L. Bullock, *J. Mater. Chem.*, 2004, **14**, 564.
21 E. Scorza, U. Birkenheuer and C. Pisani, *J. Phys. Chem.*, 1997, **107**, 9645; G. Pacchioni and P. Pescarmona, *Surf. Sci.*, 1998, **657**, 412.
22 P. V. Sushko, A. L. Shluger and C. R. A. Catlow, *Surf. Sci.*, 2000, **450**, 153.
23 A. L. Shluger, L. N. Kantorovitch, A. I. Livshits and M. J. Gillan, *Phys. Rev. B*, 1997, **56**, 15332.
24 A. M. Ferrari and G. Pacchioni, *J. Phys. Chem.*, 1995, **107**, 9645.
25 L. N. Kantorovitch, J. M. Holender and M. J. Gillan, *Surf. Sci.*, 1995, **343**, 221.
26 L. M. Molina and B. Hammer, *Phys. Rev. B*, 2004, **69**, 155424.
27 A. Bogicevic and D. R. Jennison, *Surf. Sci.*, 2002, **515**, L481.
28 S. F. Boys and F. Bernardi, *Mol. Phys.*, 1970, **19**, 553.
29 P. Pyykko, *Angew. Chem., Int. Ed.*, 2004, **43**, 4412.
30 Y. F. Zhukovskii and E. A. Kotomin, *Phys. Status Solidi C*, 2005, **2**, 347.
31 A. V. Matveev, K. M. Neuman, I. V. Yudanov and N. Rösch, *Surf. Sci.*, 1999, **246**, 123.
32 N. T. Wilson and R. L. Johnston, *Eur. Phys. J. D*, 2000, **12**, 161.
33 J. Rogan, R. Ramírez, A. H. Romero and M. Kiwi, *Eur. Phys. J. D*, 2003, **28**, 219.
34 N. Lopez and J. K. Nørskov, *J. Am. Chem. Soc.*, 2002, **124**, 11262.
35 C. Lemire, R. Meyer, S. Shaikhutdinov and H-J. Freund, *Angew. Chem., Int. Ed.*, 2004, **43**, 118.
36 J. Guzman and B. C. Gates, *J. Am. Chem. Soc.*, 2004, **126**, 2672.
37 S. Scandolo, P. Giannozzi, C. Cavazzoni, S. de Gironcoli, A. Pasquarello and S. Baroni, *Z. Kristallogr.*, 2005, **220**, 574.
38 N. Troullier and J. L. Martins, *Phys. Rev. B*, 1991, **43**, 1993.

39 S. G. Louie, S. Froyen and M. L. Cohen, *Phys. Rev. B*, 1982, **26**, 1738.
40 L. Kleinman and D. M. Bylander, *Phys. Rev. Lett.*, 1982, **48**, 1425.
41 J. M. Soler, M. R. Beltrán, K. Michaelian, I. L. Garzón, P. Ordejón, D. Sánchez-Portal and E. Artacho, *Phys. Rev. B*, 2000, **61**, 5771.
42 M. E. Straumanis, *J. Mater. Sci.*, 1988, **23**, 757.
43 C. Hampel, K. Peterson and H.-J. Werner, *Chem. Phys. Lett.*, 1992, **190**, 1.
44 S. A. Varganov, R. M. Olson and M. S. Gordon, *J. Chem. Phys.*, 2003, **119**, 2531.
45 K. P. Huber and G. Herzberg, *Molecular Spectra and Molecular Structure Constants of Diatomic Molecules*, Van Nostrand, New York, 1979.
46 U. Kaldor and B. A. Hess, *Chem. Phys. Lett.*, 1994, **230**, 1.